Revista de Metalurgia
July-September 2022, 58 (3), e223
ISSN-L: 0034-8570
https://doi.org/10.3989/revmetalm.223

Effect of boron treatment on the microstructure and toughness of Ti-containing steel weld metals

Zhan-Hang Cui, Bing-Xin Wang*

College of Mechanical Engineering, Liaoning Shihua University, Fushun 113001, China
(*Corresponding author: wangbingxin@163.com)

Submitted: 4 March 2022; Accepted: 12 September 2022; Available On-line: 19 October 2022

ABSTRACT: Ti-containing steel weld metals with boron addition contents of 0-85 ppm were prepared, and their microstructural characteristics as well as the impact toughness were investigated. The results show that in these microstructures, compared to the weld metal without boron, the addition of 22-39 ppm boron results in a remarkable increase in the amount of acicular ferrite at the expense of grain boundary ferrite, idiomorphic ferrite and side-plate ferrite. However, with a further increase in the boron content up to 61-85 ppm, the bainitic ferrite is formed, accompanied with a drop in the amount of acicular ferrite. In the acicular ferrite, the size of martensite-austenite (M/A) islands is much smaller, and the amount is much lower than those found in the bainitic ferrite. In the case of the weld metals primarily composed of acicular ferrite, during the fracture of the impact specimens, the crack propagation path is more bent in comparison with the weld metals with large amounts of grain boundary ferrite, idiomorphic ferrite, side-plate ferrite or bainitic ferrite, which that the presence of acicular ferrite improves the toughness of the weld metals. The coarse martensite-austenite islands readily induce micro-cracks at the interface between martensite-austenite islands and ferrite matrix, deteriorating the toughness. The weld metals with B contents of 22-39 ppm exhibit outstanding impact toughness because of high amount of acicular ferrite, accompanied with fine martensite-austenite islands.

KEYWORDS: Weld metal; Acicular ferrite; Boron content; Hardenability; Toughness

Citation/Citar como: Cui, Z-H.; Wang, B-X. (2022). "Effect of boron treatment on the microstructure and toughness of Ti-containing steel weld metals". *Rev. Metal.* 58(3): e223. https://doi.org/10.3989/revmetalm.223

RESUMEN: *Efecto de la adición de boro en la microestructura y tenacidad de soldaduras de acero aleado con titanio.* Se han preparado soldaduras de acero aleadas con titanio con contenidos de boro de 0-85 ppm, y se investigó su microestructura, así como su tenacidad al impacto. Los resultados muestran que, en estas microestructuras, en comparación con la soldadura sin boro, la adición de 22-39 ppm de boro da como resultado un aumento notable en la cantidad de ferrita acicular a expensas de la ferrita que se forma en el límite de grano, la ferrita idiomórfica y la ferrita de placa lateral. Sin embargo, con un mayor aumento en el contenido de boro hasta 61-85 ppm, se forma la ferrita bainítica, acompañada de una caída en la cantidad de ferrita acicular. En la ferrita acicular, el tamaño de las islas de martensita-austenita (M/A) es mucho menor, y la cantidad es inferior comparado con la que se forma en la ferrita bainítica. En el caso de las soldaduras compuestos principalmente de ferrita acicular, durante la fractura de las muestras sometidas a impacto, la ruta de propagación de la grieta muestra una ruta más zigzagueante en comparación con las soldaduras con grandes cantidades de ferrita en el límite de grano, ferrita idiomórfica, ferrita de tipo placa lateral o ferrita bainítica, lo que demuestra que la presencia de ferrita acicular mejora la tenacidad de los metales de soldadura. Las islas groseras de martensita-austenita inducen fácilmente micro-grietas en la interfaz entre las islas de martensita-austenita y la matriz de ferrita, lo que deteriora la tenacidad. Las soldaduras con contenidos de B de 22-39 ppm exhiben una excelente tenacidad al impacto debido a la alta cantidad de ferrita acicular, acompañada de finas islas de martensita-austenita.

PALABRAS CLAVE: Soldadura metálica; Ferrita acicular; Adición de boro; Templabilidad; Tenacidad

ORCID ID: ZhanHang Cui (https://orcid.org/0000-0001-7842-2148); BingXin Wang (https://orcid.org/0000-0002-2035-7344)

1. INTRODUCTION

The microstructures of low carbon low alloy steel weld metals are usually composed of different amounts of coarse-grained transformation products (i.e., grain boundary ferrite (GBF), idiomorphic ferrite (IF) and side-plate ferrite (SPF)), bainitic ferrite (BF), and fine acicular ferrite (AF), depending on the chemical compositions of weld metals, welding processes, cooling conditions, etc. The GBF and IF are the proeutectoid ferrite (PF) nucleated respectively at prior austenite grain boundaries and the inclusions within austenite (Jorge *et al*., 2021). The SPF, also known as Widmanstätten ferrite, forms from pre-existing GBF (Spanos and Hall, 1996). The microstructural constituent type plays a substantial role in determining the mechanical properties, especially the toughness of the weld metals. Compared to other ferritic phases, such as GBF, IF and SPF, AF can significantly enhance the toughness of weld metals owing to its fine-grained microstructural characteristics (Zhang *et al*., 2011; Winarto *et al*., 2020; Mosallaee and Semiromi, 2021). Therefore, AF is desirable to develop extensively in the weld metal microstructures.

AF nucleates intragranularly in the form of independent plates on the inclusions (Ricks *et al*., 1982), so the inclusion feature is a crucial factor affecting AF formation. The literatures (Wang *et al*., 2018; Zhang *et al*., 2018; Milani and Saeid, 2020; Uto *et al*., 2020) reported that some specific type Ti-containing inclusions can effectively promote AF nucleation by Mn depletion and/or crystallographic lattice match mechanisms. In addition, the hardenability of the weld metal also has a considerable effect on the AF formation (Lee and Pan, 1995) as a result of the competition relationships between AF and GBF, IF, SPF, etc., in the course of the austenite decomposition during cooling after welding (Ferrante and Farrar, 1982). The formation temperatures for GBF, IF and SPF are higher than that for AF (Farrar and Harrison, 1987) and, as a result, GBF, IF and SPF nucleate prior to AF during austenite to ferrite transformation in low hardenability weld metals (Chaveriat *et al*., 1987). For the sake of obtaining a high proportion of AF in the microstructure and the desirable mechanical properties, the hardenability of weld metal can be increased by addition of appropriate alloy elements to suppress coarse transformation products of GBF, IF and SPF. Mosallaee and Semiromi (2021) studied the influence of the Ni content on the microstructures and the mechanical properties in E7018-G electrode weld metal, and pointed that when Ni is increased up to a critical content of 1.2 wt.%, the amount of AF is enhanced from 32% to 62%, accompanied with a decrease in the amounts of IF, GBF and SPF, and accordingly, with a noticeable improvement in the tensile strength as well as the impact toughness of weld metal. Winarto *et al*. (2020) obtained similar conclusions in their works about the microstructure and impact toughness relationship for different Ni levels of the electrode in multi-pass FCA welded SM570-TMC steel joints. Additionally, also by means of adding Mo or Cr elements (Han *et al*., 2008), or increasing by Mn content (Fujiyama and Shigesato, 2021) in weld metals, the expected microstructures and mechanical properties are obtained.

Boron (B) element is another additive used to increase the hardenability, and even a small amount of B can also enhance the hardenability of the weld metal. Free B dissolved in austenite is known to segregate strongly to the austenite grain boundaries, lowering the interfacial energy. On the basis of the transformation thermodynamics, the decrease in the interfacial energy raises the energy barrier for ferrite nucleation at the austenite grain boundaries and, as a result, suppresses the transformation products preferentially nucleated at prior austenite grain boundaries, such as GBF and SPF (Mortimer and Nicholas, 1976; He *et al*., 1989; Seto *et al*., 1999; Shigesato *et al*., 2014). Consequently, the hardenability of weld metal and /or steel is enhanced (Lin and Cheng, 1987; Terzic *et al*., 2013).

In the present study, the weld metals with a certain amount of Ti, but different B contents were prepared by a submerged-arc welding process. In these weld metals, expensive elements, such as Ni and Mo, were not added, and Mn content was lower. The microstructures in the weld metals with different B contents were analyzed, and the microstructure-toughness relationship was investigated. This work aims at that in the case of no additions of Ni, Mo, etc., in the weld metals, a high amount of AF and an excellent impact toughness can also be obtained only by B addition, and the alloying cost is decreased.

2. MATERIALS AND METHODS

2.1. Weld metals preparation

Figure 1 illustrates the preparation process of the weld metals with different B contents. By a plasma arc build-up welding process, pure Fe powder was first deposited in a trapezoid slot with about 15 mm depth machined in a 20 mm thick C-Mn steel plates. Subsequently, a 7 mm deep single side V-groove was machined at the build-up welds. Finally, for the sake of obtaining the experimental weld metals, a single pass submerged-arc welding process was applied with a H08MnA welding wire of 4 mm in diameter, and the welding voltage and electric current are 30 V and 460 A, respectively. The compositions of the weld metals were adjusted by adding different amounts of B-Fe powder (21 wt.-% B) and a certain amount of Ti-Fe powder (33 wt.-% Ti) to the groove before welding. Furthermore, a small amount of Mn-Fe powder (81 wt.-% Mn) was also filled due to very low Mn content in welding wire.

The compositions of weld metals were determined by a Shimadzu OES-5500 optical emission spectrometer except for oxygen and nitrogen, which were analyzed using a Leco TC-436 N/O analyzer. The compositions of the welding wire and weld metals are listed in Table 1 and Table 2, respectively.

2.2. Microstructure analyses and tests of impact toughness

The specimens for metallographic microstructure observation were cut from the weld metals, and the examined planes were vertical to the welding direction. After mechanically polished, the specimens were etched with 4% nital solution and LePera reagent, respectively. The microstructural morphologies along with M/A islands were examined under a Leica DMIRM image analyzer, and the amounts of different ferritic phases were measured quantitatively.

According to Fig. 1, sub-size Charpy V-notch impact specimens (5 mm×10 mm×55 mm) were extracted from the welding joints, and impact tests were per-

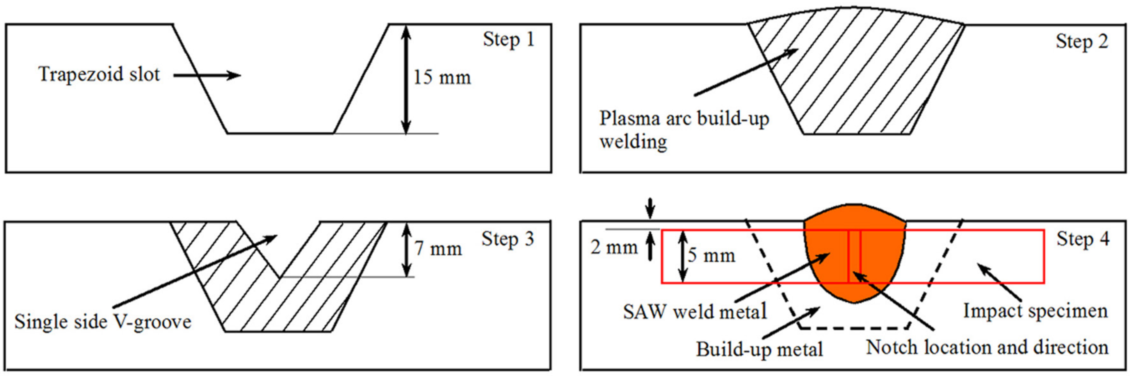

FIGURE 1. Schematic drawing showing the preparation of the weld metal.

TABLE 1. Chemical compositions of the welding wire (wt.-%)

C	Mn	Si	S	P	Al
0.05	0.86	0.06	0.022	0.02	0.01

TABLE 2. Chemical compositions of weld metals (wt.-%)

C	Mn	Si	S	P	Al	Ti	B	O	N
0.062	1.55	0.25	0.028	0.035	0.015	0.021	0	380	70
0.056	1.53	0.27	0.024	0.033	0.012	0.019	22	390	68
0.061	1.58	0.19	0.027	0.031	0.015	0.022	39	385	69
0.053	1.49	0.22	0.031	0.028	0.011	0.024	61	395	67
0.058	1.52	0.26	0.022	0.032	0.013	0.021	85	400	73

(B, O, and N: in ppm)

formed at -30 ºC by a SANTAM STM-300J machine. The average values of absorbed impact energy were calculated after five specimens were tested at every compositions point (determined by the B content).

The fracture surface and the cross-sectional region beneath the fracture surface coated by nickel were observed using an FEI Quanta 600 SEM to investigate the fracture morphology and crack propagation during fracture.

3. RESULTS AND DISCUSSION

Figure 2 indicates the metallographic microstructures in weld metals with different B contents, and the contents of ferritic phases in the microstructures are shown in Table 3. It is clearly evident that the B content has a significant effect on the weld metal microstructures. For the weld metal without B, the microstructure is composed of a series of different ferritic phases, i.e., GBF + IF (39% content), SPF (35% content) and AF (26% content). It is worth noting that these ferritic phases have a distinct difference in terms of grain size. The AF, as opposed to other ferritic phases, is finer. In the case of 22 ppm B content, the AF amount is increased to 76%, accordingly the contents of GBF+IF and SPF are decreased to 20% and 4%, respectively. In the 39 ppm B weld metal, the microstructure basically consists of AF, while other ferritic phases almost disappear. However, further increase of the B content to 61 ppm results in the appearance of BF with 41% content, accompanied by a drop of AF amount to 59%. For the weld metal with

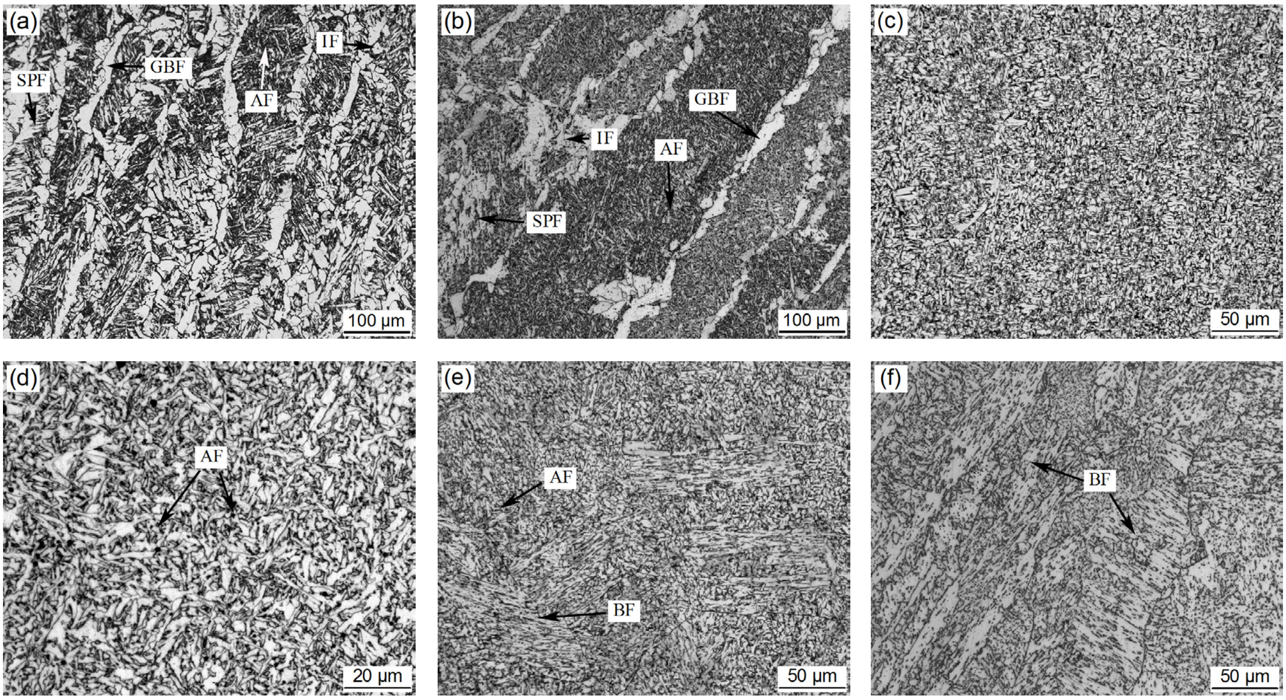

Figure 2. Metallographic microstructures of weld metals with B contents of (a) 0 ppm, (b) 22 ppm, (c) 39 ppm, (d) 39 ppm under amplification, (e) 61 ppm, and (f) 85 ppm.

Table 3. Quantitative measurements of ferritic phases in microstructures and corresponding impact toughness values

B contents	Constituents fractions (area %)				Impact absorbed energy (J)
	IF+GBF	SPF	AF	BF	
without B	39	35	26	0	35
22 ppm	20	4	76	0	67
39 ppm	0	0	100	0	75
61 ppm	0	0	59	41	45
85 ppm	0	0	0	100	23

85 ppm B, the microstructure is completely composed of BF. The authors do not have a clear explanation to why high amounts of B promote the formation of BF at the expense of AF, producing the opposite effect observed at low B levels (ferritic phases like GBF, PF or SPF as well as BF are inhibited and AF formation is promoted at inclusions). Further investigations are required in this regard.

Additionally, the B content also affects the amount and size of the M/A islands in the microstructures. The characteristics of M/A islands etched in LePera reagent are shown in Fig. 3. The M/A islands and the ferrite matrix exhibit white and grey color characteristics, respectively. Comparing this image with Figs. 2c and 2f, it can be seen from Fig. 3a that in the 39 ppm B weld metal (microstructure is dominated by AF), M/A islands have tiny size and much small amount, while M/A islands indicate opposite characteristics in the weld metal with 85 ppm B content (the microstructure is characterized by having BF).

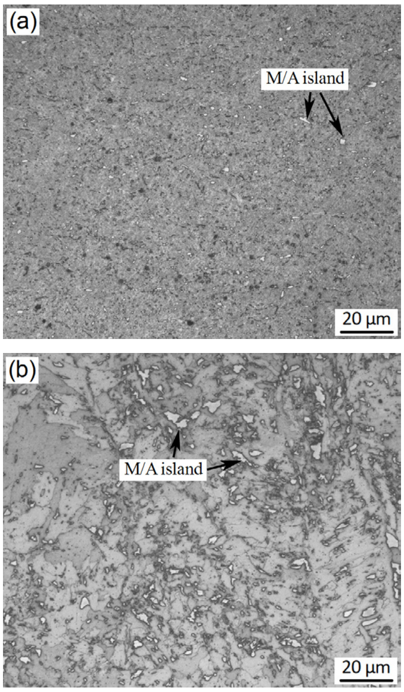

Figure 3. M/A islands characteristics in the weld metals with B contents of (a) 39 ppm and (b) 85 ppm.

In the microstructures of low carbon low alloy steel weld metals, different ferritic phases form at their specific temperature ranges during continuous cooling. The formation temperatures for IF, GBF and SPF are higher than that for AF (Farrar and Harrison, 1987), while BF usually forms at a lower temperature compared with AF (Dowling *et al.*, 1986; Jorge *et al.*, 2021). Though there are some differences in the transformation temperatures between above ferritic phases, in the case of continuous cooling after welding, two or more ferritic phases could coexist in the weld metal microstructures, as shown in Fig. 2. It is well known that in a CCT diagram, the B shifts to the right the nose of the transformation fronts of those phases nucleating at the prior austenite grain boundaries (i.e., GBF and SPF), which are phases that nucleate at higher temperatures. This facilitates the formation of other phases at lower temperatures that form intragranularly (Lin and Cheng, 1987; Terzic *et al.*, 2013). In the case of the present compositions of weld metals, the hardenability of the weld metal without B should be lower, so the austenite transforms into large amounts of IF, GBF and SPF at higher temperature ranges. In the weld metals with B addition of 22-39 ppm, the hardenability is increased, which retards the formation of GBF, IF and SPF. On the other hand, as shown in Fig. 4a, owing to containing Ti-oxides, AF nucleation is promoted, leading to a remarkable increase in the AF amount. For the 61-85 ppm B alloyed weld metals, the BF appears in the microstructures. The reason is probably that the Ti-oxides are inefficient for AF nucleation due to the changes of the Ti-oxides in the chemical compositions and constituents under high B contents, as shown in Fig. 4b. The further works should be carried out to confirm this. Moreover, as the bainite grows, the carbon is rejected outside the bainitic ferrite laths/plates, increasing locally the stability of the austenite close to these plates, which results in the appearance of large amount of M/A islands with much coarse size in the microstructure (Wen *et al.*, 2019).

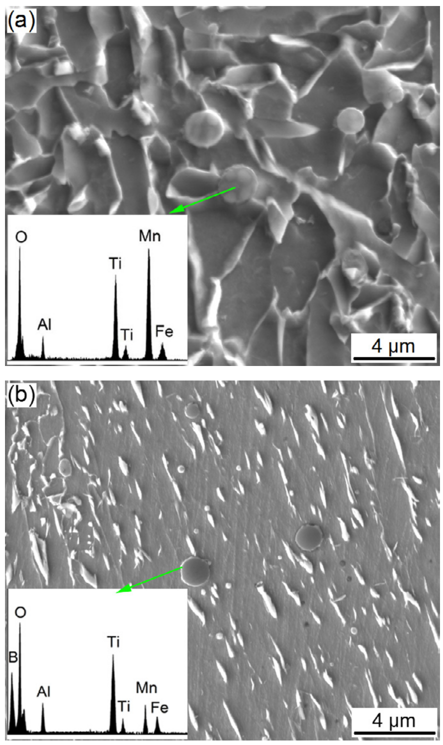

Figure 4. SEM images of (a) 39 and (b) 85 ppm B weld metal microstructures, showing different role of Ti-oxides for AF nucleation under different B contents.

Figure 5 indicates the experimental results of the impact test for the weld metals with different B contents. For the B-free weld metal, it can be seen that in addition to a small amount of dimples, a large amount of cleavage patterns are observed in the fracture surface, and the impact absorbed energy is lower. In the case of the sample with a B addition of 22-39 ppm, the fracture characteristics change from a mixture of cleavage pattern and dimple to a fully dimpled morphology. The impact absorbed energy values have increased in these weld metals, especially in 39 ppm B alloyed weld metal, for which the highest impact absorbed energy is obtained. However, further increase in the B content up to 61 ppm causes a decrease of impact absorbed energy. The fracture morphology is basically the same as that of the B-free weld metal, with the exception of having more dimples in the weld metal with a B content of 61 ppm. In the weld metal with a B content of 85 ppm, the fracture morphology exhibits a cleavage fracture with the lowest impact absorbed energy.

The impact toughness of the weld metals is closely correlated with their weld metal microstructures, as shown in Tables 3. It is clearly visible from Tables 3 that the impact toughness of the weld metals is enhanced gradually with the increase in AF amount in the microstructures.

Figure 6 shows the effect of microstructure on the crack propagation path during specimen fracture. It can

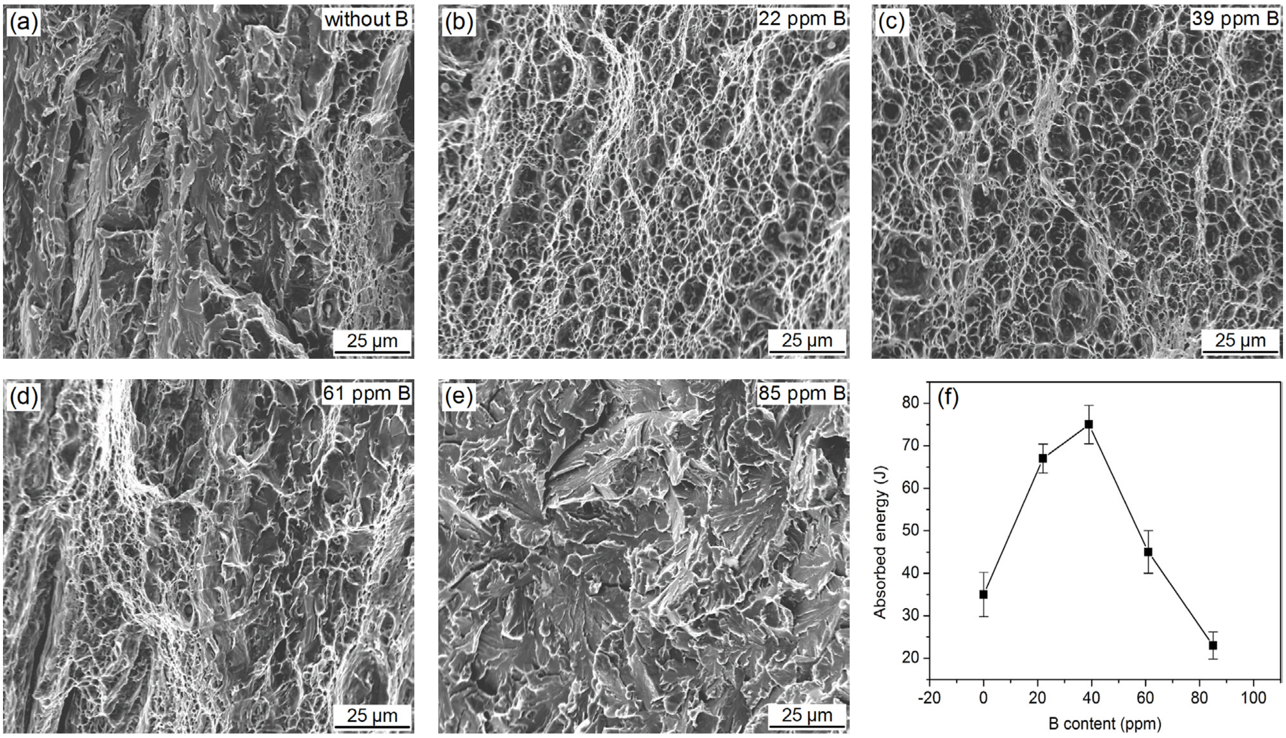

FIGURE 5. Experimental results of impact test at -30 ºC: (a)-(e) fracture morphologies and (f) impact absorbed energy.

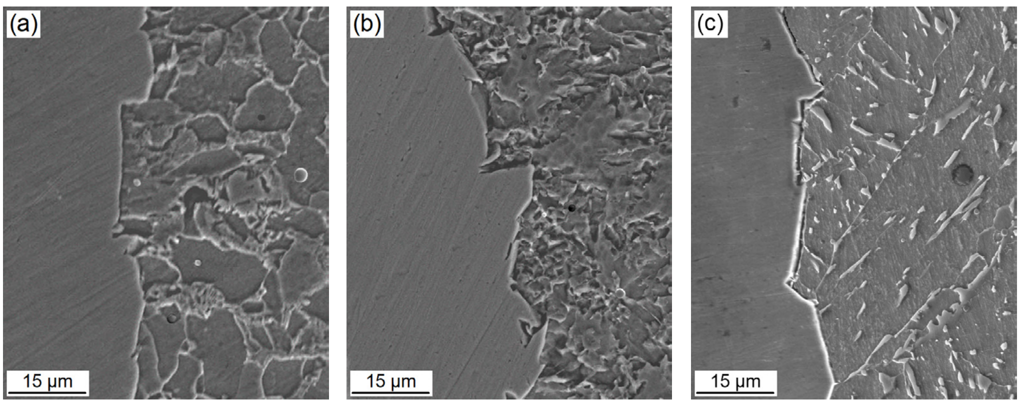

FIGURE 6. SEM images of the side surfaces of the fracture surfaces for the impact specimens (a) without B, (b) with 39 ppm B and (c) with 85 ppm B.

be seen that in the case of the microstructure containing large amounts of coarse GBF, IF and SPF (weld metal without B, Fig. 6a), or the microstructure mainly composed of BF (85 ppm B weld metal, Fig. 6c), the crack propagation path is rather straight. In contrast, for the sample with a high amount of AF in the microstructure (39 ppm B weld metal, Fig.6b), crack propagation deflects frequently and, as a result, the crack propagation path gets more bent.

AF is known to consist of fine-grained lath-like ferrite separated by the grain boundaries with the misorientation of 15° or more (i.e., high angle grain boundary) (Liu *et al*., 2017; Abson, 2018). The high angle grain boundaries (HAGBs) can efficiently hinder crack propagation, and force crack to change propagation direction during fracture (Wang *et al*., 2009). Therefore, as shown in Fig. 6b, AF can lead to a more twisty crack propagation due to its microstructure and type of grain boundaries. For the BF, low angle grain boundaries distribute between parallel arranged bainitic ferrite plates within a bainite packet with HAGBs (Wen *et al*., 2019). Thus, the crack propagates almost in a straight line manner inside a coarse bainite packet, and crack propagation direction does not deflect until it encounters bainite packet boundaries, as shown in Fig. 6c. Similar to BF, low angle grain boundaries exist between adjacent side-plate ferrites (Spanos and Hall, 1996), which can not prevent crack propagation. Although there are HAGBs between the grains of GBF and IF (Wang *et al*., 2014), the crack propagation also displays straighter path due to coarse grain, as shown in Fig. 6a.

Frequently deflecting the crack paths resulted from the impediment of HAGBs can consume more crack propagation energy, leading to an improved impact toughness (Wang *et al*., 2009). Consequently, the high amount of AF in the microstructure can increase the impact toughness of the weld metal.

Furthermore, M/A islands in the microstructure also have a significant effect on the impact toughness. Figure 7 presents that voids or microcracks usually initiate at the

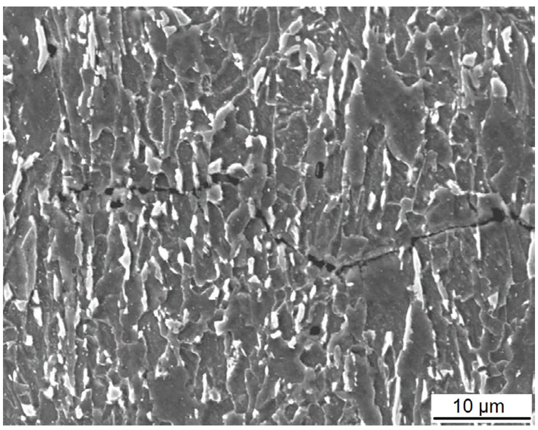

Figure 7. SEM analysis of cross-sectional area beneath fracture surface for the impact specimen with 85 ppm B.

interfaces between coarse-sized M/A islands and ferritic phases, deteriorating impact toughness. Conversely, fine M/A islands hardly cause microcracks. The literatures (Chen *et al*., 1984; Davis and King, 1994) showed that the hard M/A islands in the soft ferrite matrix can lead to a high stress concentration at the interfaces between M/A islands and ferrites under exerted load due to the distinctions of hardness and strength between these two structures, which readily induces microcracks. The size of M/A islands is a key factor for the microcracks formation induced by M/A islands (Moeinifar *et al*., 2011; Jorge *et al*., 2021). With the increase in the size of M/A islands, the exerted load for inducing the microcrack is decreased (Lan *et al*., 2014; Qin *et al*., 2019; Cui *et al*., 2020). On the other hand, the literatures (Li *et al*., 2011; Lan *et al*., 2012; Li *et al*., 2015) documented that fine-sized M/A islands do not impair the toughness of metal. As a consequence, the microstructures with a high amount AF, for example 39 ppm B alloyed weld metal, exhibit outstanding impact toughness due to the small amount of M/A islands with a fine size (as shown in Fig. 3a). On the contrary, for the microstructure characterized by having BF, for instance 85 ppm B weld metal, the impact toughness is deteriorated dramatically because of a large amount of coarse M/A islands (as shown in Fig. 3b).

4. CONCLUSIONS

– The addition of 22-39 ppm B in the steel weld metals containing Ti results in a remarkable increase in the amount of AF at the expense of GBF, IF and SPF in the microstructures. However, with further increase in the B content up to 61-85 ppm, BF is formed, accompanied with a drop in the amount of AF. In the weld metals with a mainly AF microstructure, the size of the M/A islands is much smaller, and the amount is much lower than those microstructures containing BF.
– In the case of the steel weld metals which microstructure is primarily composed of AF, the crack propagation path is more bent in comparison to the weld metals with large amounts of GBF, IF and SPF, or BF. The coarse M/A islands readily induce microcracks at the interface between M/A islands and ferrite matrix, deteriorating the toughness.
– The weld metals with B contents of 22-39 ppm exhibit excellent impact toughness because of having a high amount of AF and fine M/A islands in the microstructure.

ACKNOWLEDGMENTS

This work was financially supported by a Project of Education Department of Liaoning Province (grant Nº L2016132). Authors are grateful to Drs. H.Y. Wu and W.N. Zhang (State Key Laboratory of Rolling & Automation of Northeastern University, China) for providing helps in SEM analyses works.

REFERENCES

Abson, D.J. (2018). Acicular ferrite and bainite in C-Mn and low alloy steel arc weld metals. *Sci. Technol. Weld. Join*. 23 (8), 635-648. https://doi.org/10.1080/13621718.2018.1461992.

Chaveriat, P.F., Kim, G.S., Shah, S., Indacochea, J.E. (1987). Low carbon steel weld metal microstructures: The role of oxygen and manganese. *J. Mater. Eng*. 9 (3), 253-267. https://doi.org/10.1007/BF02834145.

Chen, J.H., Kikuta, Y., Araki, T., Yoneda, M., Matsuda, Y. (1984). Micro-fracture behaviour induced by M-A constituent (Island Martensite) in simulated welding heat affected zone of HT80 high strength low alloyed steel. *Acta Metall*. 32 (10), 1779-1788. https://doi.org/10.1016/0001-6160(84)90234-7.

Cui, J., Zhu, W., Chen, Z., Chen, L. (2020). Effect of simulated cooling time on microstructure and toughness of CGHAZ in novel high-strength low-carbon construction steel. *Sci. Technol. Weld. Join*. 25 (2), 169-177. https://doi.org/10.1080/13621718.2019.1661116.

Davis, C.L., King, J.E. (1994). Cleavage initiation in the intercritically reheated coarse-grained heat-affected zone: Part I. Fractographic evidence. *Metall. Mater. Trans. A* 25 (3), 563-573. https://doi.org/10.1007/BF02651598.

Dowling, J.M., Corbett, J.M., Kerr, H.W. (1986). Inclusion phases and the nucleation of acicular ferrite in submerged arc welds in high strength low alloy steels. *Metall. Mater. Trans. A* 17 (9), 1611-1623. https://doi.org/10.1007/BF02650098.

Farrar, R.A., Harrison, P.L. (1987). Acicular ferrite in carbon-manganese weld metals: An overview. *J. Mater. Sci*. 22 (11), 3812-3820. https://doi.org/10.1007/BF01133327.

Ferrante, M., Farrar, R.A. (1982). The role of oxygen rich inclusions in determining the microstructure of weld metal deposits. *J. Mater. Sci*. 17 (11), 3293-3298. https://doi.org/10.1007/BF01203498.

Fujiyama, N., Shigesato, G. (2021). Effects of Mn and Al on acicular ferrite formation in SAW weld metal. *ISIJ Int*. 61 (5), 1614-1622. https://doi.org/10.2355/isijinternational.ISIJINT-2020-407.

Han, F., Hwang, B., Suh, D.W., Wang, Z.C., Lee, D.L., Kim, S.J. (2008). Effect of molybdenum and chromium on hardenability of low-carbon boron-added steels. *Met. Mater. Int*. 14 (6), 667-672. https://doi.org/10.3365/met.mat.2008.12.667.

He, X.L., Chu, Y.Y., Jonas, J.J. (1989). Grain boundary segregation of boron during continuous cooling. *Acta Metall*. 37 (1), 147-161. https://doi.org/10.1016/0001-6160(89)90274-5.

Jorge, J.C.F., Souza, L.F.G., Mendes, M.C., Bott, I.S., Araujo, L.S., Dos Santos, V.R., Rebello, J.M.A., Evans, G.M. (2021). Microstructure characterization and its relationship with impact toughness of C-Mn and high strength low alloy steel weld metals - A review. *J. Mater. Res. Technol*. 10, 471-501. https://doi.org/10.1016/j.jmrt.2020.12.006.

Lan, L., Qiu, C., Zhao, D., Gao, X., Du, L. (2012). Analysis of martensite-austenite constituent and its effect on toughness in submerged arc welded joint of low carbon bainitic steel. *J. Mater. Sci*. 47 (11), 4732-4742. https://doi.org/10.1007/s10853-012-6346-x.

Lan, L., Qiu, C., Song, H., Zhao, D. (2014). Correlation of martensite-austenite constituent and cleavage crack initiation in welding heat affected zone of low carbon bainitic steel. *Mater. Lett*. 125, 86-88. https://doi.org/10.1016/j.matlet.2014.03.123.

Lee, J.L., Pan, Y.T. (1995). The formation of intragranular acicular ferrite in simulated heat-affected zone. *ISIJ Int*. 35 (8), 1027-1033. https://doi.org/10.2355/isijinternational.35.1027.

Li, C., Wang, Y., Chen, Y. (2011). Influence of peak temperature during in-service welding of API X70 pipeline steels on microstructure and fracture energy of the reheated coarse grain heat-affected zones. *J. Mater. Sci*. 46 (19), 6424-6431. https://doi.org/10.1007/s10853-011-5592-7.

Li, X., Fan, Y., Ma, X., Subramanian, S.V., Shang, C. (2015). Influence of martensite-austensite constituents formed at different intercritical temperatures on toughness. *Mater. Des*. 67, 457-463. https://doi.org/10.1016/j.matdes.2014.10.028.

Lin, H.R., Cheng, G.H. (1987). Hardenability effect of boron on carbon steels. *Mater. Sci. Technol*. 3 (10), 855-859. https://doi.org/10.1179/mst.1987.3.10.855.

Liu, D., Guo, N., Xu, C.S., Li, H., Yang, K., Feng, J. (2017). Effects of Mo, Ti and B on microstructure and mechanical properties of underwater wet welding joints. *J. Mater. Eng. Perform*. 26 (5), 2350-2358. https://doi.org/10.1007/s11665-017-2629-3.

Milani, J.M., Saeid, T. (2020). Acicular ferrite nucleation and growth in API5L-X65 steel submerged arc welded joints. *Mater. Sci. Technol*. 36 (13), 1398-1406. https://doi.org/10.1080/02670836.2020.1783774.

Moeinifar, S., Kokabi, A.H., Madaah Hosseini, H.R. (2011). Role of tandem submerged arc welding thermal cycles on properties of the heat affected zone in X80 microalloyed pipe line steel. *J. Mater. Process. Technol*. 211 (3), 368-375. https://doi.org/10.1016/j.jmatprotec.2010.10.011.

Mortimer, D.A., Nicholas, M.G. (1976). Surface and grain-boundary energies of AISI 316 stainless steel in the presence of boron. *Met. Sci*. 10 (9), 326-332. https://doi.org/10.1179/msc.1976.10.9.326.

Mosallaee, M., Semiromi, M.T. (2021). Effect of nickel content on the microstructural, mechanical and corrosion behavior of E7018-G electrode weld metal. *J. Mater. Eng. Perform*. 30 (12), 8901-8912. https://doi.org/10.1007/s11665-021-06100-9.

Qin, H., Guo, Y., Wang, L., Liang, P., Shi, Y., Cui, Y. (2019). Effect of heat inputs on microstructure and mechanical properties in CGHAZ of BWELDY960Q steel. *Kovove Mater*. 57 (5), 355-362. https://doi.org/10.4149/km_2019_5_355.

Ricks, R.A., Howell, P.R., Barritte, G.S. (1982). The nature of acicular ferrite in HSLA steel weld metals. *J. Mater. Sci*. 17 (3), 732-740. https://doi.org/10.1007/BF00540369.

Seto, K., Larson, D., Warren, P., Smith, G.D. (1999). Grain boundary segregation in boron added interstitial free steels studied by 3-dimensional atom probe. *Scr. Mater*. 40 (9), 1029-1034. https://doi.org/10.1016/S1359-6462(98)00485-0.

Shigesato, G., Fujishiro, T., Hara, T. (2014). Grain boundary segregation behavior of boron in low-alloy steel. *Metall. Mater. Trans. A* 45 (4), 1876-1882. https://doi.org/10.1007/s11661-013-2155-3.

Spanos, G., Hall, M.G. (1996). The formation mechanism(s), morphology, crystallography of ferrite sideplates. *Metall. Mater. Trans. A* 27 (6), 1519-1534. https://doi.org/10.1007/BF02649812.

Terzic, A., Calcagnotto, M., Guk, S., Schulz, T., Kawalla, R. (2013). Influence of boron on transformation behavior during continuous cooling of low alloyed steels. *Mater. Sci. Eng. A* 584, 32-40. https://doi.org/10.1016/j.msea.2013.07.010.

Uto, K., Nakayama, K., Kisaka, Y., Kimura, F., Terasaki, H. (2020). A study on the acicular ferrite formation in steel weld metals for gas metal arc welding. *Quarterly Journal of the Japan Welding Society* 38 (2), 6-10. https://doi.org/10.2207/qjjws.38.6s.

Wang, W., Shan, Y. Yang, K. (2009). Study of high strength pipeline steels with different microstructures. *Mater. Sci. Eng*. A 502 (1-2), 38-44. https://doi.org/10.1016/j.msea.2008.10.042.

Wang, B.X., Lian, J.B., Liu, X.H., Wang, G.D. (2014). Effect of ultra-fast cooling on microstructure and mechanical properties in a plain low carbon steel. *Kovove Mater*. 52 (3), 135-140. https://doi.org/10.4149/km_2014_3_135.

Wang, B., Liu, X., Wang, G. (2018). Inclusion characteristics and acicular ferrite nucleation in Ti-containing weld metals of X80 pipeline steel. *Metall. Mater. Trans. A*. 49 (6), 2124-2138. https://doi.org/10.1007/s11661-018-4570-y.

Wen, C., Deng, X., Tian, Y., Wang, Z., Misra, R.D.K. (2019). Microstructural evolution and toughness of the various HAZs in 1300-MPa-grade ultrahigh-strength structural steel. *J. Mater. Eng. Perform*. 28 (3), 1301-1311. https://doi.org/10.1007/s11665-019-3869-1.

Winarto, W., Oktadinata, H., Siradj, E.S., Priadi, D., Baskoro, A.S., Ito, K. (2020). Microstructure and impact toughness relationship for different nickel level of electrode in multi-pass FCA welded SM570-TMC steel joint. *Quarterly Journal of the Japan Welding Society* 38 (2), 154-158. https://doi.org/10.2207/qjjws.38.154s.

Zhang, L., Li, Y., Wang, J., Jiang, Q. (2011). Effect of acicular ferrite on cracking sensibility in the weld metal of Q690+Q550 high strength steels. *ISIJ Int*. 51 (7), 1132-1136. https://doi.org/10.2355/isijinternational.51.1132.

Zhang, C.J., Gao, L.N., Zhu, L.G. (2018). Effect of inclusion size and type on the nucleation of acicular ferrite in high strength ship plate steel. *ISIJ Int*. 58 (5), 965-969. https://doi.org/10.2355/isijinternational.ISIJINT-2017-696.